INTERNATIONAL JOURNAL FOR NUMERICAL METHODS IN FLUIDS, VOL. 6, 275–290 (1986)

COMPARISON BETWEEN TWO FINITE-DIFFERENCE SCHEMES FOR COMPUTING THE FLOW AROUND A CYLINDER

A. BORTHWICK*

Department of Civil Engineering, University of Salford, Salford, U.K.

SUMMARY

Separated flow past a circular cylinder is computed from two finite-difference Navier–Stokes models. Stream functions are calculated using a successive-over-relaxation (SOR) procedure. Alternating-direction-implicit (ADI) and 'upwind' directional difference explicit (DDE) numerical schemes for solving the vorticity-transport equation are compared. The 'upwind' differencing technique produces artificial viscosity which damps the wake and suppresses vortex shedding. It is shown to be unreliable and so the ADI approach is recommended.

INTRODUCTION AND BRIEF REVIEW OF LITERATURE

Navier–Stokes finite-difference models of flow past a cylinder have a long history, originating well before the invention of computers. The earliest formulation was given by Thom[1] in 1933 in which he solved arithmetically the viscous flow equations in two dimensions by means of succesive approximations. Uniform flow past a circular cylinder at Reynolds numbers 10 and 20 was examined.

Using a log-polar co-ordinate transformation Kawaguti[2] transformed the flow field onto a rectangular mesh and integrated numerically the vorticity transport form of the Navier–Stokes equations at a Reynolds number of 40. Central differencing approximations to the vorticity-transport and stream function equations were applied at all node points. Computers were not generally available in 1953 and so Kawaguti carried out the computations by hand.

Time-dependent solutions for the earliest stages of impulsively started symmetric flow at Reynolds numbers of 40 and 100 and from 1 to 100 were calculated by Payne[3] and Kawaguti and Jain,[4] respectively. In 1964, Fromm[5] produced a numerical solution for unsteady incompressible flow past rectangular obstacles at Reynolds numbers up to 6000.

A directional difference scheme for non-linear advective terms in the vorticity-transport equation and a hybrid mesh structure designed to fit the local flow conditions were devised by Thoman and Szewczyk[6,7] and used to present time-dependent solutions for a wide range of Reynolds numbers from 1 to 10^6 for stationary and rotating cylinders. Asymmetric perturbations were added so that alternate vortex shedding would occur behind the cylinder.

Son and Hanratty[8] examined impulsively started symmetric flow at Reynolds numbers up to 500. At every iteration the vorticity-transport equation was solved by splitting each time step into two half steps and solving the two systems of simultaneous equations, formed by

* Lecturer

0271–2091/86/050275–16$08.00

Received 26 April 1985
Revised 25 November 1985

central-difference approximations to the flow equations with implicit directional weightings. This was based on an alternating-direction-implicit (ADI) method proposed by Peaceman and Rachford.[9] No mention is made as to why Son and Hanratty chose the more rigorous ADI technique to obtain updated vorticity values. An implicit Crank–Nicolson type integration was used by Collins and Dennis[10] who attempted to examine the development of steady wakes for very high Reynolds numbers. They found that for Reynolds numbers greater than 100 the procedure broke down after some time and failed to converge. For higher Reynolds numbers the integration procedure broke down at early times before an expected secondary vortex appeared.

Rather more attention has been focused on unsteady flow solutions, especially where vortex shedding is evident. Ta Phuoc Loc[11] analysed the growth of primary and secondary vortices at Reynolds numbers of 300, 500 and 1000. He used a second-order ADI method to solve the vorticity-transport equation. Although the flow did not reach a stage where vortices were shed, Ta Phuoc Loc demonstrated the unsteady nature of the secondary vortices in the wake at early flow times. His numerical results agreed with experimental measurements and indicated that the ADI technique could be applicable to high Reynolds number flows. Many numerical models, such as those given by Jordan and Fromm,[12] Jain and Rao,[13] Jain and Goel,[14] Patel,[15] Lin, Pepper and Lee[16] and Martinez[17] have been devised to show the unsteady wake developed behind a cylinder. They showed that vortex shedding occurs at Reynolds numbers above a critical value close to 80. All these authors used simple meshes which restricted the applicable range of Reynolds numbers to 400 and under. Jordan and Fromm tried to model a flow at Reynolds number 1000, but their mesh was too coarse and they obtained unrepresentative results. Jain and Rao and Jain and Goel used straightforward central-differencing to describe the vorticity-transport equation with the result that their results were restricted to low Reynolds numbers below 200. Martinez used the ADI method and a technique similar to Patel based on Fourier analysis to solve the time-dependent equation and obtained satisfactory results up to a Reynolds number of 200. Generally, their work agreed with experimental observations.

Lin, Pepper and Lee[16] conducted a survey of three numerial schemes that had been proposed by other authors. First, they discussed the DDE-GSI scheme suggested by Thoman and Szewczyk[6,7] in which the vorticity-transport equation was solved by a direction-difference (DDE) method and then the stream functions were calculated using a Gauss–Seidel iteration (GSI) process. Second, they examined the ADI-SOR method which used an alternating-direction-implicit scheme and a successive-over-relaxation procedure to obtain updated values of vorticity and stream functions, respectively. They finally studied a strongly implicit procedure (SIP-SIP) method which uses a technique of matrix factorization and elimination to solve both equations. They observed that the SIP-SIP and ADI-SOR methods gave better accuracy than the DDE-GSI method and that the SIP-SIP method was more economical than the ADI-SOR approach as regards computer time.

Although Lin, Pepper and Lee[16] mentioned that the streamline patterns obtained by the DDE-GSI method deviated noticeably from those obtained by the other two methods they did not elucidate as to what exactly these differences were. They did note that the separation angles predicted by the DDE-GSI scheme used by Thoman and Szewczyk[6,7] were larger than measured values and predictions by other authors. Unfortunately, they did not indicate that the DDE-GSI method leads to the creation of artificial viscosity which rapidly destroys the vorticity away from the cylinder and effectively curtails vortex-shedding at all Reynolds numbers.

Many authors, such as Martinez,[17] Son and Hanratty[8] and Lin and Lee[18] have compared the effect of mesh sizes and outer boundary conditions for solutions of the Navier–Stokes equations. A detailed discussion of the relative merits of different conditions has been given by

Roache.[19] Most of the authors mentioned in this brief review have given the subject of boundary conditions careful attention.

It is the purpose of this paper to examine in detail ADI-SOR and DDE-SOR methods for predicting flow around a cylinder.

FUNDAMENTAL EQUATIONS

In polar co-ordinates, the Navier–Stokes equations are given by continuity and momentum considerations in an inertial frame of reference as

$$\operatorname{div}\mathbf{q} = V_r + r\frac{\partial V_r}{\partial r} + \frac{\partial V_\theta}{\partial \theta} = 0, \tag{1}$$

where

$$\mathbf{q} = \begin{Bmatrix} V_r \\ V_\theta \end{Bmatrix},$$

$$\rho\left[\frac{\partial V_r}{\partial t} + V_r\frac{\partial V_r}{\partial r} + \frac{V_\theta}{r}\frac{\partial V_r}{\partial \theta} - \frac{V_\theta^2}{r}\right] = \frac{-\partial P}{\partial r} + \mu\left[\frac{1}{r}\frac{\partial}{\partial r}\left(r\frac{\partial V_r}{\partial r}\right) + \frac{1}{r^2}\frac{\partial^2 V_r}{\partial \theta^2} - \frac{V_r}{r^2}\frac{2}{r^2}\frac{\partial V_\theta}{\partial \theta}\right] \tag{2}$$

and

$$\rho\left[\frac{\partial V_\theta}{\partial t} + V_r\frac{\partial V_\theta}{\partial r} + \frac{V_\theta}{r}\frac{\partial V_\theta}{\partial \theta} + \frac{V_\theta V_r}{r^2}\right] = \frac{-1}{r}\frac{\partial P}{\partial \theta} + \mu\left[\frac{1}{r}\frac{\partial}{\partial r}\left(r\frac{\partial V_\theta}{\partial r}\right) + \frac{1}{r^2}\frac{\partial^2 V_\theta}{\partial \theta^2} - \frac{V_\theta}{r^2} + \frac{2}{r^2}\frac{\partial V_r}{\partial \theta}\right], \tag{3}$$

where ρ is the fluid density and μ is the fluid kinematic viscosity.

The vorticity-transport equation is obtained from the (r, θ) momentum equations (2) and (3) by cross-differentiating the radial momentum equation with respect to θ and the angular momentum equation with respect to r (after multiplying by r) and substituting in the vorticity. The velocity components V_r and V_θ are defined as

$$V_r = \frac{1}{r}\frac{\partial \psi}{\partial \theta} \quad \text{and} \quad V_\theta = \frac{-\partial \psi}{\partial r}. \tag{4}$$

The vorticity, ω, is defined as

$$\omega = \frac{1}{r}\left[\frac{\partial (rV_\theta)}{\partial r} - \frac{\partial V_r}{\partial \theta}\right]. \tag{5}$$

The parabolic vorticity-transport equation is obtained as

$$\frac{\partial \omega}{\partial t} + \frac{1}{r}\frac{\partial (V_\theta \omega)}{\partial \theta} + \frac{1}{r}\frac{\partial (rV_r\omega)}{\partial r} = \nu\left[\frac{1}{r}\frac{\partial}{\partial r}\left(r\frac{\partial \omega}{\partial r}\right) + \frac{1}{r^2}\frac{\partial^2 \omega}{\partial \theta^2}\right], \tag{6}$$

where the fluid kinematic viscosity $\nu = \mu/\rho$; and the stream function equation is

$$\frac{\partial^2 \psi}{\partial r^2} + \frac{1}{r}\frac{\partial \psi}{\partial r} + \frac{1}{r^2}\frac{\partial^2 \psi}{\partial \theta^2} = -\omega. \tag{7}$$

In order to non-dimensionalize the equations, the following non-dimensional quantities are introduced for flow past an infinitely long cylinder of radius r_a:

$$r' = r/r_a, \quad V'_r = V_r/U_\infty, \quad V'_\theta = V_\theta/U_\infty, \tag{8}$$

$$t' = tU_\infty/r_a \quad \text{and} \quad P' = \frac{P - P_\infty}{\rho U_\infty^2}, \quad \text{etc.}$$

Three non-dimensional numbers are defined as:

$$\text{Reynolds number, } Re = \frac{2U_\infty r_a}{\nu}, \tag{9}$$

$$\text{Keulegan-Carpenter number, } K_c = \frac{\pi U_\infty}{\Omega r_a} \tag{10}$$

and

$$\text{Strouhal number, } S = \frac{2fr_a}{U_\infty}, \tag{11}$$

where Ω is angular velocity and f is the vortex shedding frequency.

Using these parameters equations (4), (5), (6) and (7) are rewritten in dimensionless form. The transformation

$$r' = e^{az}; \qquad z = \frac{1}{a}\ln r', \tag{12}$$

$$\theta' = a\theta; \qquad \theta = \frac{1}{a}\theta', \tag{13}$$

results in simplification of the previous equations and allows the use of a regular mesh for the numerial treatment of the equations. From now on the primes are dropped for convenience. Hence the equations become

$$V_r = E_z^{-1/2}\frac{\partial \psi}{\partial \theta}, \qquad V_\theta = -E_z^{-1/2}\frac{\partial \psi}{\partial z}, \tag{14}$$

$$E_z\frac{\partial \omega}{\partial t} + \frac{\partial \omega}{\partial z}\frac{\partial \psi}{\partial \theta} - \frac{\partial \omega}{\partial \theta}\frac{\partial \psi}{\partial z} = \frac{2}{Re}\left[\frac{\partial^2 \omega}{\partial z^2} + \frac{\partial^2 \omega}{\partial \theta^2}\right] \tag{15}$$

and

$$\frac{\partial^2 \psi}{\partial z^2} + \frac{\partial^2 \psi}{\partial \theta^2} = -E_z\omega, \tag{16}$$

where $E_z = a^2 e^{2az}$.

NUMERICAL SCHEME

The log-polar transformation leads to a regular 'rectangular' mesh which lends itself to simple numerical treatment. The discretized domain is shown in Figure 1.

The choice of the various discretization parameters has to be undertaken carefully in order to gain the best results. Too fine a mesh produces a wasteful, time-consuming computer simulation,

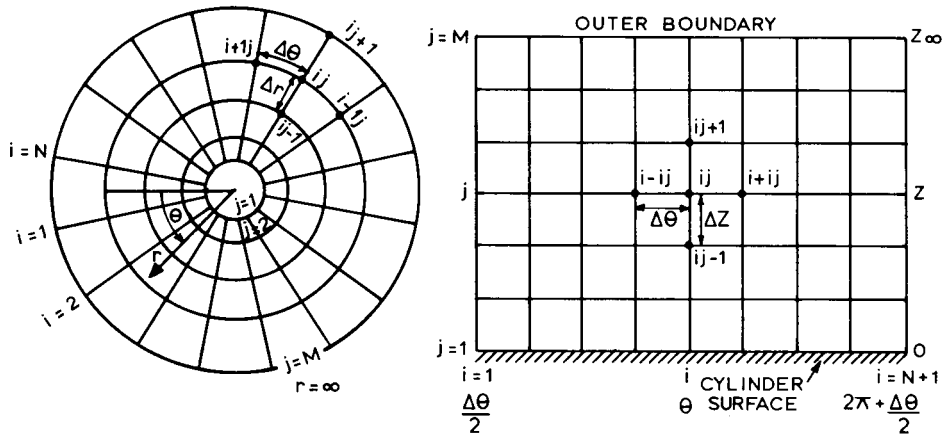

Figure 1. Discretization of domain

whereas if it is too coarse, the results are inaccurate or unstable. A number of authors, notably Lin and Lee,[18] Son and Hanratty,[8] Martinez[17] and Thoman and Szewczyk[6,7] have produced comparisons of results obtained for grids with various spacings of Δz and $\Delta\theta$. They found that the presence of at least one grid point within the boundary layer is essential for a meaningful model.

Thoman and Szewczyk[6,7] derived a limiting condition for the time step incorporating diffusion and convective vorticity transport conditions. This was based on an analysis which combined the Neumann stability criterion and the Courant condition. It should be noted, however, that precision and stability contrive to run against each other. Thus, a diminution in grid cell size can result in a reduction in time step in order to preserve stability for a fixed Reynolds number.

The discretization parameters used here are

$$\Delta t = 0{\cdot}02 \quad \text{and} \quad \Delta z = \Delta\theta = \pi/45.$$

Martinez[17] studied the influence of the location of the outer boundary on the near wake. From his work, it was decided to ensure that the outer boundary, r_∞, was located at a distance greater than $80r_a$ from the centre of the cylinder (where r_a is the cylinder radius).

A brief outline of the procedure for solving the flow equations as used in the computer programs is given in the flow diagram presented in Figure 2.

SOLUTION OF THE STREAM FUNCTION EQUATION

In terms of second-order accurate central difference approximations at each node the stream function equation can be rewritten and rearranged to give

$$\psi_{ij} := \left\{ E_z\omega_{ij} + \frac{\psi_{i\,j+1}}{\Delta z^2} + \frac{\psi_{i\,j-1}}{\Delta z^2} + \frac{\psi_{i+1\,j}}{\Delta\theta^2} + \frac{\psi_{i-1\,j}}{\Delta\theta^2} \right\} \Big/ \left(\frac{2}{\Delta z^2} + \frac{2}{\Delta\theta^2} \right). \tag{17}$$

Thus, a new updated value of the stream function, ψ_{ij}, can be obtained at each node using the values from the four surrounding nodes. Equation (17) forms the basis of the iterative scheme in which the continuity equation is assumed satisfied when the difference between the new and old values of stream function is less than a predetermined error parameter $\varepsilon = 10^{-3}$. The iterative process is accelerated by the use of a successive over-relaxation parameter Ω_s where

$$\psi_{ij} := \psi_{ij} - \Omega_s(\psi_{ij}^{(1)} - \psi_{ij}), \tag{18}$$

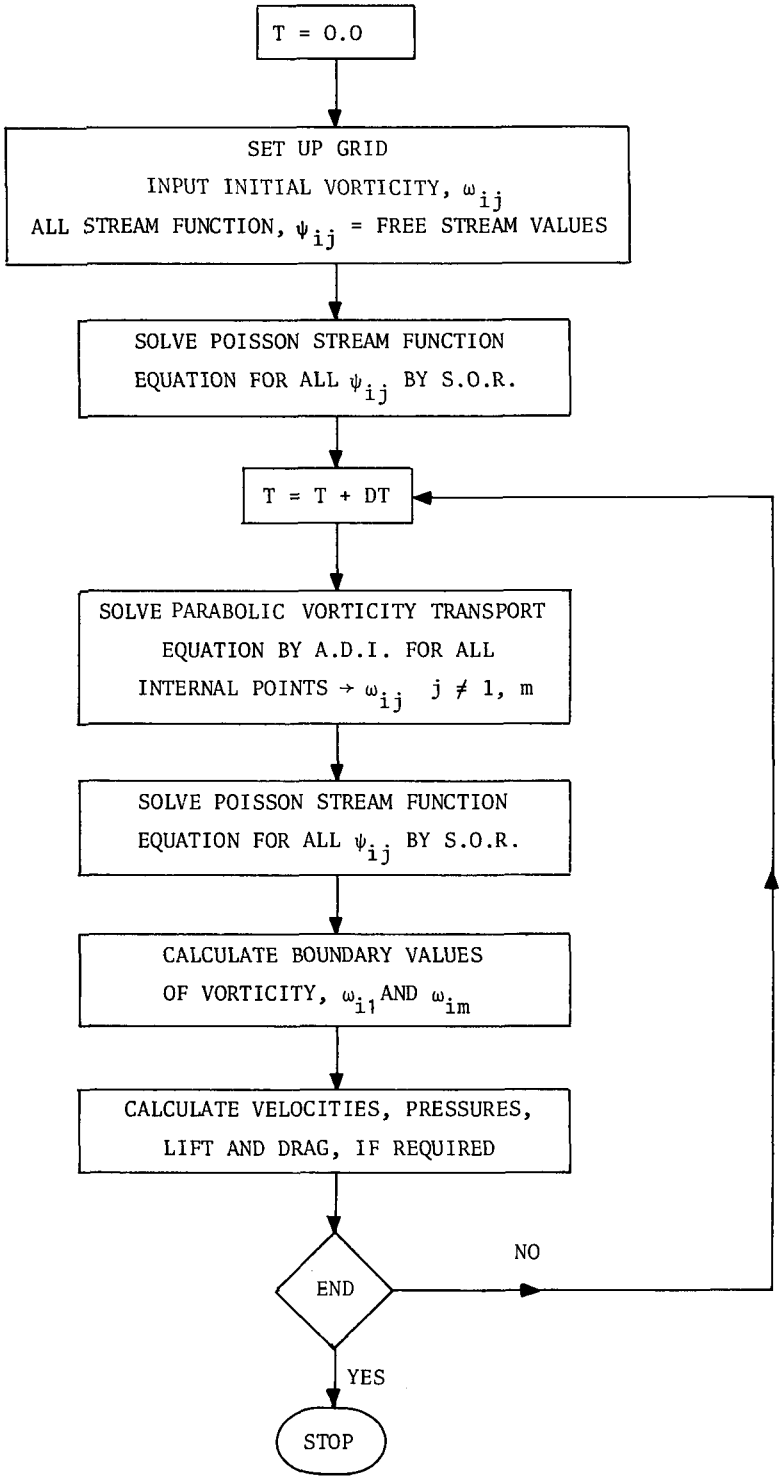

Figure 2. Flow chart indicating numerical scheme

where $\psi_{ij}^{(1)}$ is the result of applying equation (17). An optimum value of $\Omega_s = 1.72$ was used throughout.

SOLUTION OF THE VORTICITY-TRANSPORT EQUATION

A simple central differencing approximation to the vorticity-transport equation gives unstable results except for the lowest Reynolds numbers. Therefore 'upwind' directional difference (DDE) and alternating-direction-implicit (ADI) schemes are implemented.

The 'Upwind' directional differencing formulation

Rearranging equation (15), and using the directional difference explicit (DDE) method, as discussed by Thoman and Szewczyk,[6,7] in which forward differencing was used for the $\partial\omega/\partial t$ term, directional differences for the advective terms and central differences for the diffusion terms, the vorticity-transport equation is solved to give

$$\omega_{ij}^{k+1} = \omega_{ij} + \frac{\Delta t}{E_z}\left\{\frac{2}{Re}\left[\frac{\omega_{i\,j+1}^k + \omega_{i\,j-1}^k - 2\omega_{ij}^k}{\Delta z^2} + \frac{\omega_{i+1\,j}^k + \omega_{i-1\,j}^k - 2\omega_{ij}^k}{\Delta\theta^2}\right]\right.$$
$$-\left[\left(\frac{\partial\psi}{\partial\theta}\omega\right)_{i\,j+\frac{1}{2}}^k - \left(\frac{\partial\psi}{\partial\theta}\omega\right)_{i\,j-\frac{1}{2}}^k\right]\frac{1}{\Delta z}$$
$$\left.+\left[\left(\frac{\partial\psi}{\partial z}\omega\right)_{i+\frac{1}{2}\,j}^k - \left(\frac{\partial\psi}{\partial z}\omega\right)_{i-\frac{1}{2}\,j}^k\right]\frac{1}{\Delta\theta}\right\}, \tag{19}$$

where the superscripts k and $k+1$ refer to the time levels.

This method has been used elsewhere to remedy numerical instabilty, but it introduces an artificial viscosity which results in first-order accuracy only. Thoman and Szewczyk[6,7] chose it because for very high Reynolds numbers it was the only method of six they examined which did not require prohibitively small cells to achieve calculational stability.

Alternating-direction-implicit formulation

In the ADI method equation (15) is decoupled numerically by first 'releasing' the equation in the θ-direction while holding the z-components 'fixed', and secondly, 'releasing' the equation in the z-direction with the θ-component 'fixed'. Hence, the following pair of equations is obtained:

$$\frac{Re}{2}\left[E_z\frac{\omega^{k+1/2}-\omega^k}{\Delta t/2} - \left(\frac{\partial\psi}{\partial z}\right)^k\left(\frac{\partial\omega}{\partial\theta}\right)^{k+1/2}\right] - \left(\frac{\partial^2\omega}{\partial\theta^2}\right)^{k+1/2} = -\frac{Re}{2}\left(\frac{\partial\psi}{\partial\theta}\frac{\partial\omega}{\partial z}\right)^k + \left(\frac{\partial^2\omega}{\partial z^2}\right)^k \tag{20a}$$

and

$$\frac{Re}{2}\left[E_z\frac{\omega^{k+1}-\omega^{k+1/2}}{\Delta t/2} + \left(\frac{\partial\psi}{\partial\theta}\right)^k\left(\frac{\partial\omega}{\partial z}\right)^{k+1}\right] - \left(\frac{\partial^2\omega}{\partial z^2}\right)^{k+1} = \frac{Re}{2}\left(\frac{\partial\psi}{\partial z}\right)^k\left(\frac{\partial\omega}{\partial\theta}\right)^{k+1/2} + \left(\frac{\partial^2\omega}{\partial\theta^2}\right)^{k+1/2} \tag{20b}$$

Equations (20) are approximated using a central difference scheme. With some rearranging the following equations can be derived:

$$-\omega_{i-1\,j}^{k+1/2}\left[1 - \alpha\left(\frac{\partial\psi}{\partial z}\right)_{ij}^k\right] + \omega_{ij}^{k+1/2}[2 + \lambda E_z] - \omega_{i+1\,j}^{k+1/2}\left[1 + \alpha\left(\frac{\partial\psi}{\partial z}\right)_{ij}^k\right] = S^k, \tag{21a}$$

$$-\omega_{ij-1}^{k+1}\left[1+\beta\left(\frac{\partial\psi}{\partial\theta}\right)_{ij}^{k}\right]+\omega_{ij}^{k+1}\left[2+\frac{\lambda}{\mu}E_z\right]-\omega_{ij+1}^{k+1}\left[1-\beta\left(\frac{\partial\psi}{\partial\theta}\right)_{ij}^{k}\right]=S^{k+1}, \quad (21b)$$

where

$$S^k=\mu\left\{\omega_{ij-1}^{k}\left[1+\beta\left(\frac{\partial\psi}{\partial\theta}\right)_{ij}^{k}\right]+\omega_{ij}^{k}\left[\frac{\lambda}{\mu}E_z-2\right]+\omega_{ij+1}^{k}\left[1-\beta\left(\frac{\partial\psi}{\partial\theta}\right)_{ij}^{k}\right]\right\}, \quad (21c)$$

$$S^{k+1}=\frac{1}{\mu}\left\{\omega_{i-1j}^{k+1/2}\left[1-\alpha\left(\frac{\partial\psi}{\partial z}\right)_{ij}^{k}\right]+\omega_{ij}^{k+1/2}[\lambda E_z-2]+\omega_{i+1j}^{k+1/2}\left[1+\alpha\left(\frac{\partial\psi}{\partial z}\right)_{ij}^{k}\right]\right\} \quad (21d)$$

and

$$\alpha=\frac{\Delta\theta Re}{4},\quad \beta=\frac{\Delta z Re}{4},\quad \lambda=\frac{\Delta\theta^2 Re}{\Delta t},\quad \mu=\frac{\Delta\theta^2}{\Delta z^2}.$$

A tridiagonal system of linear equations has thus been obtained. It is solved by factorization.

The convection terms in the vorticity-transport equation are approximated here using central differences, and so the spatial accuracy is of order $(\Delta\theta^2, \Delta z^2)$ which is better than that of order $(\Delta\theta, \Delta z)$ given by 'upwind' differencing. The ADI method gives the time based derivatives to second-order accuracy as long as the parameters $\partial\psi/\partial\theta$ and $\partial\psi/\partial z$ are evaluated at the correct instant.

In order to construct the tridiagonal matrices, the boundary conditions must be considered. The first directional release requires the implementation of a boundary condition along the axis where $\theta=0$ (or $\theta=2\pi$). It is self evident that $\omega_{N+1\,j}=\omega_{ij}$ in the log-polar co-ordinate system shown in Figure 1. With the aid of this condition it is possible to set up a matrix of the form

$$\begin{bmatrix} b_1 & -c_1 & & & & \\ -a_2 & b_2 & -c_2 & & & \\ & & \vdots & & & \\ & & -a_i & b_i & -c_i & \\ & & & & \vdots & \\ & & & & -a_N & b_N \end{bmatrix}\begin{bmatrix}\omega_{1j}\\ \omega_{2j}\\ \vdots\\ \omega_{ij}\\ \vdots\\ \omega_{Nj}\end{bmatrix}=\begin{bmatrix}K_1^*\\ K_2^*\\ \vdots\\ K_i^*\\ \vdots\\ K_N^*\end{bmatrix}, \quad (22)$$

using equation (22) given before, where

$$b_1=2+\lambda E_z,\quad c_1=1+\alpha\left(\frac{\partial\psi}{\partial z}\right)_{ij}^{k},\quad K_1^*=S^k+\omega_{Nj}^{k+1/2}\left[1-\alpha\left(\frac{\partial\psi}{\partial z}\right)_{ij}^{k}\right],$$

$$a_i=1-\alpha\left(\frac{\partial\psi}{\partial z}\right)_{ij}^{k},\quad b_i=2+\lambda E_z,\quad c_i=1+\alpha\left(\frac{\partial\psi}{\partial z}\right)_{ij},\quad K_i^*=S^k,$$

$$a_N=1-\alpha\left(\frac{\partial\psi}{\partial z}\right)_{Nj}^{k},\quad b_N=2+\lambda E_z \quad\text{and}\quad K_N^*=S^k+\omega_{1j}^{k+1/2}\left[1+\alpha\left(\frac{\partial\psi}{\partial z}\right)_{Nj}^{k}\right]. \quad (23)$$

The fictitious vorticities $\omega_{Nj}^{k+1/2}$ and $\omega_{ij}^{k+1/2}$ contained in the expressions for K_1^* and K_N^*, respectively, are not known beforehand and so they are replaced by the lagged values ω_{Nj}^{k} and ω_{1j}^{k}. This assumption is reasonable for low values of j because it is applied using values taken from positions in the mesh close to the cylinder where successive values of vorticity alter least in the majority of cases. Using recursion formulae and Cholesky decomposition the matrix system given in equation (22) can be solved for the intermediate fictitious vorticities $\omega_{ij}^{k+1/2}$.

The second directional sweep requires the surface and outer boundary conditions to be implemented. These are discussed later. The shortened matrix given below is constructed.

$$\begin{bmatrix} b_2 & -c_2 & & & & \\ -a_3 & b_3 & -c_3 & & & \\ & & \vdots & & & \\ & & -a_j & b_j & -c_j & \\ & & & & \vdots & \\ & & & & -a_{m-1}b_{m-1} \end{bmatrix} \begin{bmatrix} \omega_{i2} \\ \omega_{i3} \\ \vdots \\ \omega_{ij} \\ \vdots \\ \omega_{i\,M-1} \end{bmatrix} = \begin{bmatrix} K_2^* \\ K_3^* \\ \vdots \\ K_j^* \\ \vdots \\ K_{M-1}^* \end{bmatrix}, \tag{24}$$

where

$$a_2 = 2 + \frac{\lambda}{\mu}E_z, \quad c_2 = 1 - \beta\left(\frac{\partial\psi}{\partial\theta}\right)_{i2}^k, \quad K_2^* = S_2^{k+1} + \omega_{i1}\left[1 + \beta\left(\frac{\partial\psi}{\partial\theta}\right)_{i2}^k\right],$$

$$\omega_{i1} = -\frac{2\psi_{i2}}{\Delta z^2} + V_{\theta i1}, \quad a_j = 1 + \beta\left(\frac{\partial\psi}{\partial\theta}\right)_{ij}^k, \quad b_j = 2 + \frac{\lambda}{\mu}E_z,$$

$$c_j = 1 - \beta\left(\frac{\partial\psi}{\partial\theta}\right)_{ij}^k, \quad K_j^* = S^{k+1}, \quad a_{M-1} = 1 + \beta\left(\frac{\partial\psi}{\partial\theta}\right)_{i\,M-1}^k,$$

$$b_{M-1} = 1 + \frac{\lambda}{\mu}E_z + \beta\left(\frac{\partial\psi}{\partial\theta}\right)_{i\,M-1}^k \quad \text{and} \quad K_{M-1}^* = S^{k+1}. \tag{25}$$

The updated values of vorticity ω_{ij}^{k+1} are finally obtained by solving equation (24) in the same way as equation (22). The ADI process is now complete.

CALCULATION OF VELOCITIES

Using central difference approximations the radial and tangential velocity components, given in equation (14), become

$$V_{rij} = \frac{\psi_{i+1\,j} - \psi_{i-1\,j}}{2\Delta\theta E_z^{1/2}} \tag{26a}$$

and

$$V_{\theta ij} = -\frac{\psi_{i\,j+1} - \psi_{i\,j-1}}{2\Delta z E_z^{1/2}}. \tag{26b}$$

INITIAL CONDITIONS

Before the time-dependent numerical computations are started it is essential to specify initial values of vorticity and stream function throughout the grid. In flow problems of this type it is sensible to input potential flow solutions as starting conditions. For the uniform flow case, the well-known potential flow result is,

$$\psi_{ij}^* = -\left[Ur\sin\theta\left(1 - \frac{1}{r^2}\right)\right]_{ij}, \tag{27}$$

where the free stream velocity $U = 1$ and $\omega_{ij}^* = 0$

BOUNDARY CONDITIONS

A careful choice of boundary conditions is essential for the numerical scheme to produce results of physical significance without making excessive demands on the particular computer used.

Sometimes more exact conditions lead to gross costs in computer time and so it is necessary to find a sensible balance between the two constraints. This decision relies often on experience. The size and shape of mesh also have great influence on the ability of the numerical scheme to model the flow behaviour. For example, the mesh is a finite approximation to an unbounded domain and in this regular scheme the mesh is too coarse to model boundary layers properly. Thus, the boundary conditions must be applied with consideration to the mesh characteristics.

Assuming a uniform vorticity gradient $\partial\omega/\partial z = 0$ the outer boundary vorticity is given by the equation

$$\omega_{iM} = \omega_{i\,M-1}. \tag{28}$$

On the axis where $\theta = 0$ or 2π the values of the stream function ψ and the vorticity ω are not fixed and there is a displacement of the upstream line $\psi = 0$ (noticeable in uniform flows) which is expressed by a periodic oscillation of the upstream stagnation point. This displacement results from circulation produced by the alternate vortex shedding mechanism. Jordan and Fromm[12] developed a correction which takes account of this displacement and is added to the uniform flow stream function ψ^*_{iM} to give the outer boundary stream function ψ_{iM}. However, this correction was fond to produce almost the same numerical results as for the simple fixed boundary conditions. Thus

$$\psi_{iM} = \psi^*_{iM}. \tag{29}$$

A forward difference approximation is made to the angular velocity at the outer boundary, giving,

$$V_{\theta iM} = -E_z^{-1/2}\frac{\psi_{iM} - \psi_{i\,M-1}}{\Delta z}. \tag{30a}$$

The radial velocity is given in central difference form as

$$V_{riM} = \frac{\psi_{i+1\,M} - \psi_{i-1\,M}}{2\Delta\theta E_z^{1/2}}. \tag{30b}$$

A simple condition for the surface boundary condition is derived by considering the stream function equation in polar co-ordinate form. At the cylinder surface it simplifies to give

$$\omega_{i1} = V_{\theta i1} - \left.\frac{\partial^2\psi}{\partial z^2}\right|_{i1}. \tag{31}$$

The stream function second derivative is expressed in central difference form. Assuming that the stream function inside the cylinder, ψ_{i0}, is the mirror image of the stream function around the cylinder ψ_{i2} because of zero gradient

$$\omega_{i1} = V_{\theta i1} - \frac{2\psi_{i2}}{\Delta z^2}. \tag{32}$$

For uniform flow past a stationary cylinder (with no slip) the surface boundary stream function, radial and tangential velocities are fixed to give

$$\psi_{i1} = V_{ri1} = V_{\theta i1} = 0. \tag{33}$$

CALCULATION OF SURFACE PRESSURE

In order to evaluate the surface pressures the momentum components of the governing Navier–Stokes equations given by expressions (2) and (3) must be reconsidered. The pressure at a large

distance from the cylinder (i.e. the outer boundary) is assumed to be zero. The radial momentum components are converted to log-polar form, rearranged and rewritten in finite-difference notation as

$$p_{ij}^{k+1} = p_{i\,j+1}^{k+1} + \rho\,\Delta z\left[E_z^{1/2}\frac{V_{r_{ij}}^{k+1} - V_{r_{ij}}^{k}}{\Delta t} + V_{r_{ij}}^{k+1}\left(\frac{V_{r_{i\,j+1}}^{k+1} - V_{r_{i\,j-1}}^{k+1}}{2\,\Delta z}\right)\right.$$
$$\left. + V_{\theta_{ij}}^{k+1}\left(\frac{V_{r_{i+1\,j}}^{k+1} - V_{r_{i-1\,j}}^{k+1}}{2\,\Delta\theta}\right) - V_{\theta_{ij}}^{k+1}V_{\theta_{ij}}^{k+1}\right] + \frac{2\,\Delta z\,\rho}{Re\,E_z^{1/2}}\left[\frac{V_{r_{i\,j+1}}^{k+1} + V_{r_{i\,j-1}}^{k+1} - 2V_{r_{ij}}^{k+1}}{\Delta z^2}\right.$$
$$\left. + \frac{V_{r_{i+1\,j}}^{k+1} + V_{r_{i-1\,j}}^{k+1} - 2V_{r_{ij}}^{k+1}}{\Delta\theta^2} - V_{r_{ij}}^{k+1} - \frac{V_{\theta_{i+1\,j}}^{k+1} - V_{\theta_{i-1\,j}}^{k+1}}{\Delta\theta}\right] \tag{34}$$

It is now possible to step in from the outer boundary where $P_{1M} = 0$ and obtain an estimate of the surface pressure P_{11} close to the forward stagnation point.

The tangential component of the Navier–Stokes equation at the cylinder surface can be simplified by some manipulation and rewritten in log-polar form to give

$$\frac{\partial P}{\partial\theta} = \frac{2}{Re}\frac{\partial\omega}{\partial z}. \tag{35}$$

In finite-difference form this becomes

$$P_{i+1} = P_i + \frac{\Delta\theta}{Re}\left[\left.\frac{\partial\omega}{\partial z}\right|_{i+1} + \left.\frac{\partial\omega}{\partial z}\right|_{i}\right]. \tag{36}$$

Using a third-order Lagrange polynomial the relevant vorticity gradients at the surface can be obtained from

$$\left.\frac{\partial\omega}{\partial z}\right|_{i} = \frac{1}{16\,\Delta z}[-35\omega_{i1} + 70\omega_{i2} - 56\omega_{i3} + 26\omega_{i4} - 5\omega_{i5}] \tag{37}$$

and

$$\left.\frac{\partial\omega}{\partial z}\right|_{i+1} = \frac{1}{16\,\Delta z}[-35\omega_{i+1\,1} + 70\omega_{i+1\,2} - 56\omega_{i+1\,3} + 26\omega_{i+1\,4} - 5\omega_{i+1\,5}]. \tag{38}$$

Computation of the surface pressure can now take place using the value of P_{11} already specified and stepping around the cylinder in an anticlockwise direction.

DRAG AND LIFT COEFFICIENTS

The drag and lift coefficients, C_d and C_L, respectively, are obtained by performing the following integrations using a Simpson's rule numerical approximation:

$$C_d = -\int_0^{2\pi} P\cos\theta\,d\theta - \frac{2}{Re}\int_0^{2\pi}\omega\sin\theta\,d\theta, \tag{39}$$

$$C_L = -\int_0^{2\pi} P\sin\theta\,d\theta + \frac{2}{Re}\int_0^{2\pi}\omega\cos\theta\,d\theta. \tag{40}$$

COMPARISON BETWEEN ADI AND 'UPWIND' DIFFERENCING METHODS

Lin, Pepper and Lee[16] made comparisons between two implicit methods and an 'upwind' differencing scheme. Although they mentioned that the 'upwind' differencing approach gave

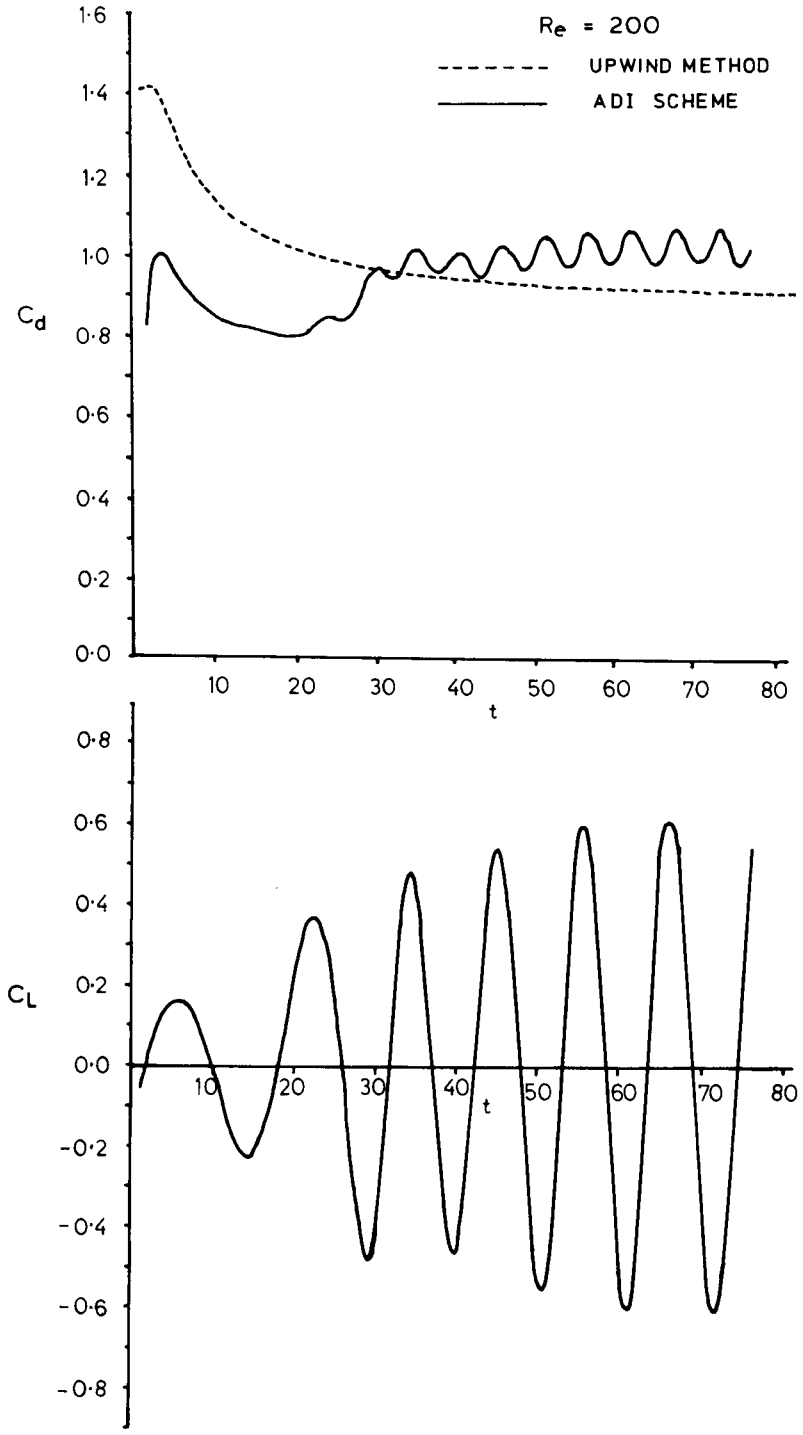

Figure 3. Lift and drag coefficients for $Re = 200$ using both upwind differencing and A.D.I. schemes

different results from those expected, they did not comment further on the method and did not present the data they obtained.

The results given here show categorically that the 'upwind' differencing scheme is unsuitable. Figure 3 charts the development of the drag and lift coefficients with time for uniform flow past a stationary cylinder at a Reynolds number of 200. The 'upwind' differencing scheme gives a drag coefficient which decays from an initially high value to a constant close to 0·9 and a lift coefficient which is negligible throughout. The results computed from the ADI scheme show that the drag coefficient decays for some time after the impulsive start, then increases somewhat and settles to a sinusoidal variation about a mean value of 1·02, whereas the lift coefficient eventually describes a sinusoid of amplitude of 0.61, centred at zero. The difference in results is a direct consequence of the excessive numerical damping due to artificial viscosity which is imposed on the flow by the 'upwind' differencing method. This is further illustrated by the stream function and vorticity contours in Figures 4 and 5. Figure 4 shows the contours obtained at a time $t = 65$ using the

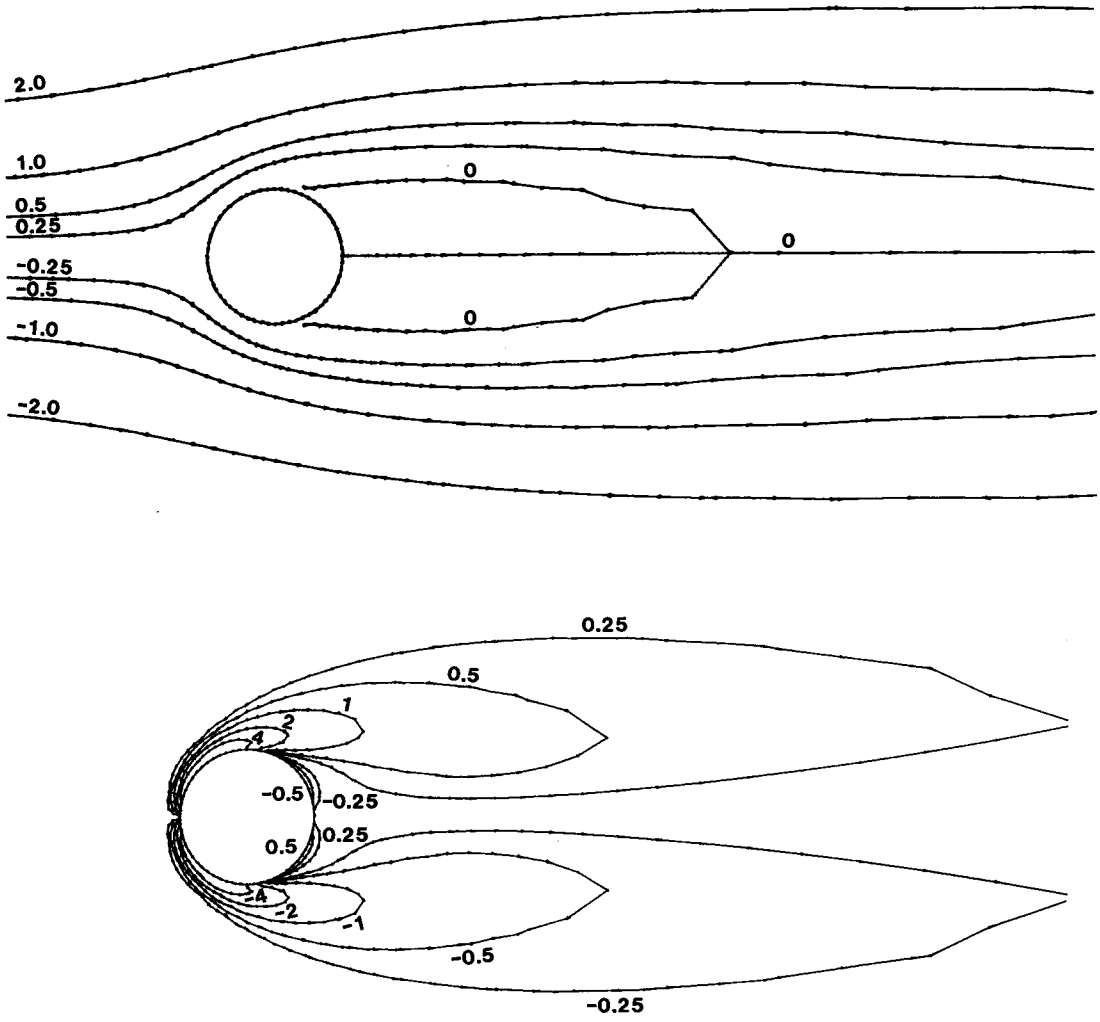

Figure 4. Stream function and vorticity contours for $Re = 200$ at $t = 65$ using upwind differencing scheme

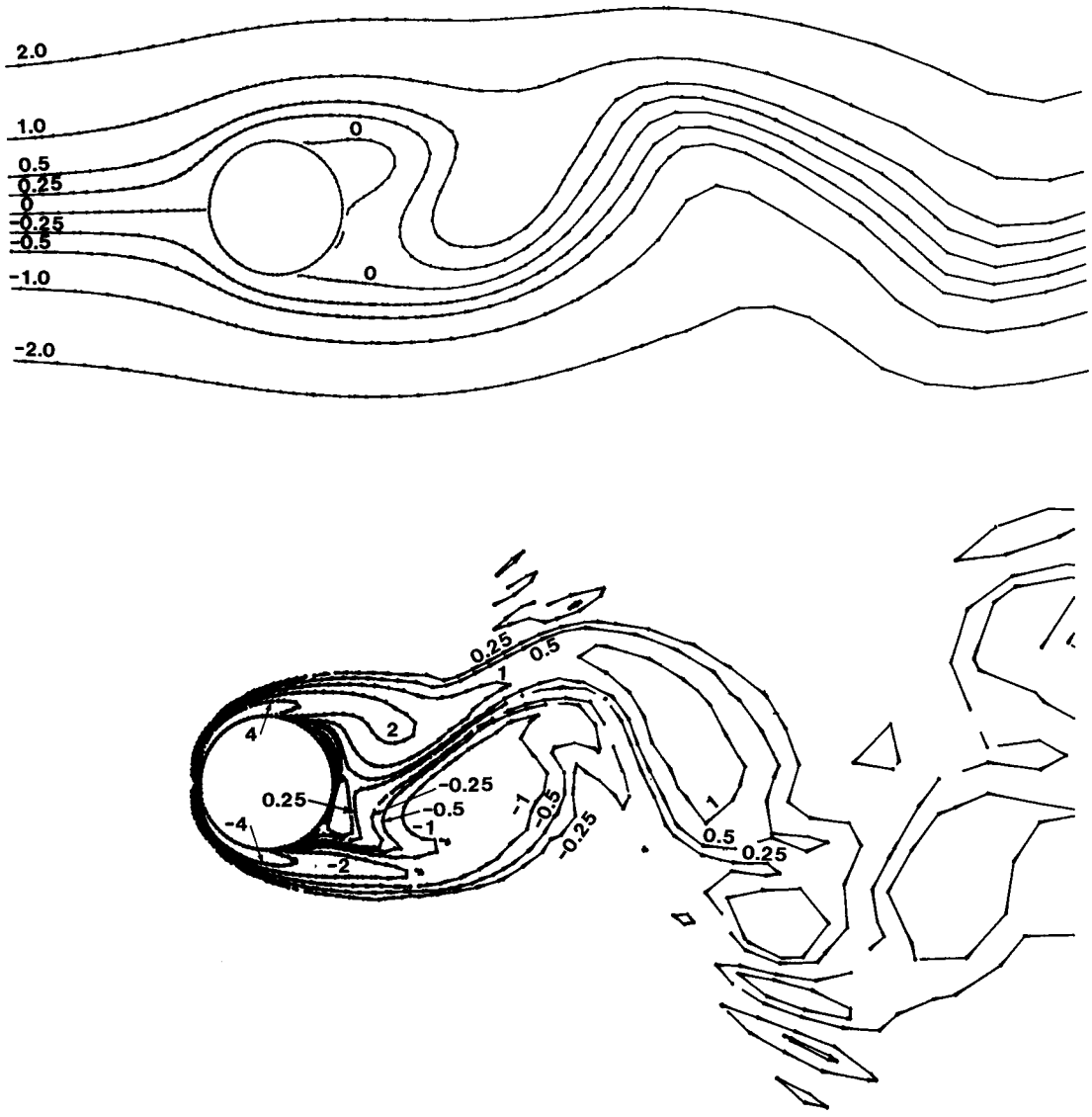

Figure 5. Stream function and vorticity contours for $Re = 200$ at $t = 65$ using A.D.I. scheme

'upwind' differencing approach. There is no vortex shedding, just a symmetric pair of Föppl vortices behind the cylinder as would be produced experimentally at a much lower Reynolds number of 60, say. The plots obtained from the ADI scheme, given in Figure 5, show that vortex shedding occurs, leading to the establishment of a von Karman vortex street in the wake, in concurrence with experimental data[20] at a Reynolds number of 200.

The results obtained at time $t = 65$, using the 'upwind' differencing approach, are summarized in Table I. It should be noted that the separation angles θ_1 and θ_2 are measured clockwise and anticlockwise, respectively, from the forward stagnation point. The separation angles were determined from the surface vorticity distribution. In no case was vortex shedding evident.

Table I. Upwind differencing scheme results

Reynolds Number Re	Separation angles θ_1	θ_1	Drag coeffficient C_d	Lift coefficient C_L
40	131·0	131·0	1·492	0·0
80	122·6	122·6	1·098	0·0
100	119·9	119·9	1·008	0·0
200	112·5	112·5	0·907	0·0
400	106·9	106·9	0·956	0·0

Table II. ADI scheme results

Reynolds Number Re	Separation angles θ_1	θ_2	Drag coefficient C_d	Lift coefficient C_L
40	126·3	126·3	1·507	0·0
80	118·4 ± 0·9	118·3 ± 0·9	1·275 ± 0·005	± 0·17
100	116·5 ± 1·4	116·1 ± 1·3	1·215 ± 0·01	± 0·26
200	111·5 ± 4·3	111·3 ± 4·3	1·02 ± 0·04	± 0·61
400	107·1 ± 7·0	106·5 ± 6·2	1·5 ± 0·12	± 1·2

Table II contains the equivalent results for the ADI scheme. Vortex shedding occurs at all Reynolds numbers greater than 80, in accordance with experimental data.

A brief examination of both Tables I and II is sufficient to show the substantial disagreement between the methods.

A hybrid mesh has also been developed by the author.[21] It was used to determine whether the 'upwind' differencing method could induce vortices to detach from the cylinder at high Reynolds numbers. Artificial triggering, as suggested by Thoman and Szewczyk[6,7] in which the cylinder was given sudden forward and backward rotations, was used in an attempt to initiate the shedding process. However, no vortex shedding could be initiated; even at a Reynolds number as high as 40,000.

CONCLUSIONS

The first-order 'upwind' differencing (DDE) method recommended by Thoman and Szewczyk[6,7] gives unsatisfactory results regardless of numerical perturbations or the type of mesh selected. Artificial viscosity generated by the scheme damps the flow and prevents vortices detaching from behind the cylinder. First order 'upwind' differencing is therefore unsuitable for this type of separated flow computation.

Implicit methods for solving the vorticity-transport equation such as the alternating-direction-implicit (ADI) scheme are recommended instead. The ADI method does not create artificial viscosity and so provides a more realistic model of laminar fluid flow situations. It may be applied to more complicated problems than uniform flow past a cylinder. For example, Borthwick[21] used the ADI-SOR technique to simulate orbital flow past a cylinder.

ACKNOWLEDGEMENTS

The author gratefully acknowledges Dr. J. R. Chaplin (of Liverpool University), Marinetech North West and the U.K. S.E.R.C. for their support in producing this work.

REFERENCES

1. A. Thom, 'The flow past cylinders at low speeds', *Proc. Roy. Soc., A*, **141,** 651 (1933).
2. M. Kawaguti, 'Numerical solution of the Navier–Stokes equations for the flow around a circular cylinder at Reynolds number 40', *J. Phys. Soc. Japan*, **8,** (6), 747 (1953).
3. R. B. Payne, 'Calculations of unsteady viscous flow past a circular cylinder', *J. Fluid Mech.*, **4,** 81 (1958).
4. M. Kawaguti and P. Jain, 'Numerical study of flow past a circular cylinder', *J. Phys. Soc. Japan*, **21,** 2055–2062 (1966).
5. J. E. Fromm, 'The time dependent flow of an incompressible viscous fluid', in *Methods in Computational Physics, Vol. III*, Academic Press, 1964, pp. 345–383.
6. D. C. Thoman, 'Numerical solutions of time dependent two-dimensional flow of a viscous incompressible fluid over stationary and rotating cylinders', *Ph.D. Thesis*, Dept. of Mech. Eng., University of Notre Dame, Indiana, August 1964.
7. D. C. Thoman and A. A. Szewczyk, 'Time-dependent viscous flow over a circular cylinder', *Physics of Fluids Supplement*, **12,** 76–86 (1969).
8. J. S. Son and T. J. Hanratty, 'Numerical solution of the flow around a cylinder at Reynolds numbers of 40, 200 and 500', *J. Fluid Mech.*, **35,** 369–386 (1969).
9. D. W. Peaceman and H. H. Rachford, Jr., 'The numerical solution of parabolic and elliptic differential equations', *Journal of the Society of Industrial and Applied Mathematics*, **3,** 28–41 (1955).
10. W. M. Collins and S. C. R. Dennis, 'Flow past an impulsively started circular cylinder', *J. Fluid Mech.*, **60,** Pt. 1, 105–127 (1973).
11. Ta Phuoc Loc, 'Numerical analysis of unsteady secondary vortices generated by an impulsively started circular cylinder', *J. Fluid Mech.*, **100,** Pt. 1, 111–128 (1980).
12. S. K. Jordan and J. E. Fromm, 'Oscillatory Drag, lift, and torque on a circular cylinder in a uniform flow', *The Physics of Fluids*, **15,** (3), 371 (1972).
13. P. C. Jain and K. S. Rao, 'Numerical solution of unsteady viscous incompressible fluid flow past a circular cylinder', *Physics of Fluids Supplement II*, **12,** 57 (1969).
14. P. C. Jain and B. S. Goel, 'Shedding of vortices behind a circular cylinder', *Computers and Fluids*, **4,** 137–142 (1976).
15. V. A. Patel, 'Time-dependent solutions of the viscous incompressible flow past a circular cylinder by the method of series truncation', *Computers and Fluids*, **4,** 13–27 (1976).
16. C. Lin, D. Pepper and S. Lee, 'Numerical methods for separated flow solutions around a circular cylinder', *AIAA Journal*, **14,** (7), 900–907 (1976).
17. G. Martinez, 'Caracteristiques dynamiques et thermiques de l'ecoulement autour d'un cylindre circulaire a nombres de Reynolds moderes', *Doctor-Ingeniuer Thesis*, L'Institute National Polytechnique de Toulouse, France, June 1979.
18. C. L. Lin and S. C. Lee, 'Transient state analysis of separated flow around a sphere', *International Journal of Computer and Fluids*, **1,** 235–250 (1973).
19. P. J. Roache, *Computational Fluid Dynamics*, Hermosa Publishers, Albuquerque, N.M., 1972, p. 434.
20. T. Sarpkaya and M. De St. Q. Isaacson, *The Mechanics of Wave Forces on Offshore Structures*, Van Nostrand Rheinold, 1981.
21. A. Borthwick, 'Orbital flow past a cylinder', *Ph.D. Thesis*, University of Liverpool, July 1982.